Accepted Manuscript

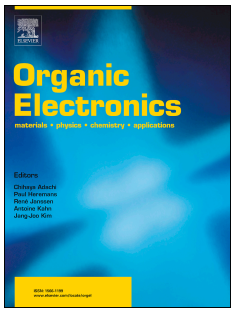

Environmentally friendly preparation of nanoparticles for organic photovoltaics

Xun Pan, Anirudh Sharma, Desta Gedefaw, Renee Kroon, Amaia Diaz de Zerio, Natalie P. Holmes, A.L. David Kilcoyne, Matthew Barr, Adam Fahy, Melissa Marks, Xiaojing Zhou, Warwick Belcher, Paul C. Dastoor, Mats R. Andersson

PII: S1566-1199(18)30262-3

DOI: 10.1016/j.orgel.2018.05.040

Reference: ORGELE 4700

To appear in: *Organic Electronics*

Received Date: 21 February 2018

Revised Date: 26 April 2018

Accepted Date: 28 May 2018

Please cite this article as: X. Pan, A. Sharma, D. Gedefaw, R. Kroon, A. Diaz de Zerio, N.P. Holmes, A.L.D. Kilcoyne, M. Barr, A. Fahy, M. Marks, X. Zhou, W. Belcher, P.C. Dastoor, M.R. Andersson, Environmentally friendly preparation of nanoparticles for organic photovoltaics, *Organic Electronics* (2018), doi: 10.1016/j.orgel.2018.05.040.

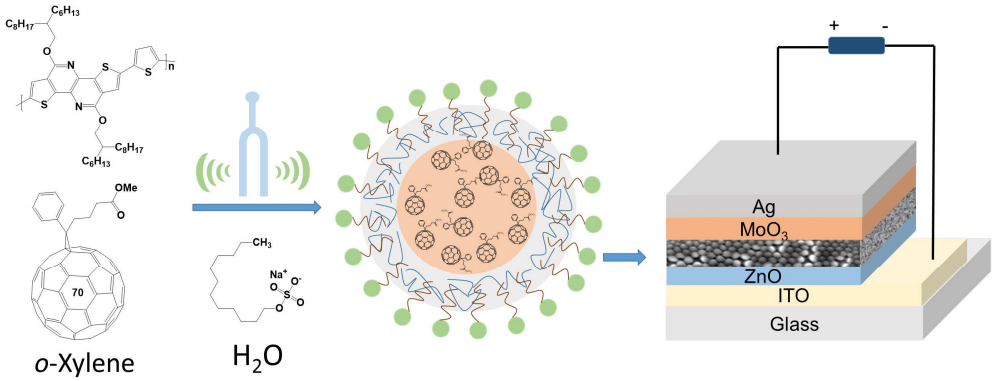

Environmentally friendly preparation of nanoparticles for organic photovoltaics

Xun Pan[a], Anirudh Sharma[a,c], Desta Gedefaw[b], Renee Kroon[d], Amaia Diaz de Zerio[d], Natalie P. Holmes[e], A. L. David Kilcoyne[f], Matthew Barr[e], Adam Fahy[e], Melissa Marks[e], Xiaojing Zhou[e], Warwick Belcher[e], Paul C. Dastoor[e], Mats R. Andersson[a,*]

[a] *Flinders Centre for Nanoscale Science and Technology, Flinders University, Sturt Road, Bedford Park, Adelaide, SA 5042, Australia*

[b] *School of Biological and Chemical Sciences, The University of South Pacific, Laucala Campus, Suva, Fiji*

[c] *Laboratoire de Chimie des Polymères Organiques (LCPO), Université de Bordeaux, UMR 5629, B8, Allée Geoffroy Saint Hilaire, 33615 Pessac Cedex, France*

[d] *Department of Chemical and Biological Engineering, Chalmers University of Technology, 41296 Göteborg, Sweden*

[e] *Centre for Organic Electronics, University of Newcastle, University Drive, Callaghan NSW 2308, Australia*

[f] *Advanced Light Source, Lawrence Berkeley National Laboratory, Berkeley, CA 94720, USA*

Abstract

Aqueous nanoparticle dispersions were prepared from a conjugated polymer poly(2,5-thiophene-alt-4,9-bis(2-hexyldecyl)-4,9-dihydrodithieno[3,2-c:3',2'-h][1,5]naphthyridine-5,10-dione) (PTNT) and fullerene blend utilizing chloroform as well as a non-chlorinated and environmentally benign solvent, *o*-xylene, as the miniemulsion dispersed phase solvent. The nanoparticles (NPs) in the solid-state film were found to coalesce and offered a smooth surface topography upon thermal annealing. Organic photovoltaics (OPVs) with photoactive layer processed from the nanoparticle dispersions prepared using chloroform as the miniemulsion dispersed phase solvent were found to have a power conversion efficiency

(PCE) of 1.04%, which increased to 1.65% for devices utilizing NPs prepared from *o*-xylene. Physical, thermal and optical properties of NPs prepared using both chloroform and *o*-xylene were systematically studied using dynamic mechanical thermal analysis (DMTA) and photoluminescence (PL) spectroscopy and correlated to their photovoltaic properties. The PL results indicate different morphology of NPs in the solid state were achieved by varying miniemulsion dispersed phase solvent.

Keywords

Nanoparticles; Organic photovoltaics; Green solvent; Environmentally friendly processing

1. Introduction

Ever increasing global energy consumption has led to a tremendous rise in fossil fuel emissions, resulting in air pollution and global warming.[1] The urgent need for the development of clean and renewable energy sources has attracted immense attention of both scientific and industrial researchers.[2-3] Undoubtedly, solar energy is one of the best candidates to fulfil the current and future energy needs.[4-5] Organic photovoltaics (OPVs) enjoy significant advantages over traditional solar technology due to their lightweight, flexibility, ease of manufacturing, scalability and low cost.[6-9] Continued research into OPV technology has led to significant improvements in the device performance with power conversion efficiency (PCE) of up to 13% being reported.[10] However, OPVs are commonly prepared via spin-coating the active materials on small indium tin oxide (ITO) coated glass substrates from non-environmentally friendly halogenated solvents,[11] which is counterproductive to achieving scalable and environmentally friendly fabrication of OPVs.

In recent years a number of publications have focussed on developing alternative OPV fabrication methods, which are scalable at low cost such as roll-to-roll printing. [8, 12-14] Although remarkable success has been achieved in printing OPVs on flexible substrates, most of the best performing materials used for printing are still processed from chlorinated solvents such as *ortho*-dichlorobenzene (*o*-DCB).[15] The large-scale use of chlorinated solvents is harmful to human health and has a detrimental impact on the environment.[16-17] Moreover, the usage of chlorinated solvents increases the cost of large-scale fabrication of OPVs, which results from expensive halogenated solvent recovery systems. The harmfulness and high cost of chlorinated solvents used for processing photoactive materials in OPV fabrication is one of the main hurdles to be overcome before the knowhow of fabricating high performing OPVs can be transferred from a lab-scale to an industrial scale fabrication. Thus, it is of utmost importance to develop green deposition methods by utilizing benign and non-chlorinated solvents.[18-20]

OPVs with active layers processed from a water or alcohol based nanoparticle dispersion has been reported in recent years.[21-24] These nanoparticles are processed from donor-acceptor blends either through a miniemulsion process with the presence of surfactant[25-28] or a precipitation method[21-23, 29]. Furthermore, conjugated polymer nanoparticles were also reported to be synthesized by direct Suzuki-Miyaura dispersion polymerization.[30-32] In the miniemulsion method, the organic solvent utilized to dissolve the active materials should ideally have high vapour pressure as well as be immiscible with water. Most procedures reported in the literature to date use harmful chlorinated solvents, such as chloroform ($CHCl_3$)[21, 33], chlorobenzene[34] or *o*-DCB[26]. Compared to conventional bulk heterojunction (BHJ) OPV fabrication, the NP method is still environmentally superior considering (a) the volume of chlorinated solvents utilized is comparably less; (b) the roll-to-roll printing of solar cells is free from chlorinated solvents as they can be removed in a closed loop system prior to

printing. Considering that the upscaling of OPVs with NP active layers will lead to an increase in the consumption of solvents used to prepare NPs, it is timely to consider the use of industrially relevant solvents during the preparation of the NPs of the photoactive materials in addition to the subsequent deposition.

In this paper, we report for the first time the preparation of water-dispersed nanoparticles using a relatively benign and industrially relevant solvent, *o*-xylene, as the miniemulsion dispersed phase solvent, and successfully demonstrate the fabrication of solar cells with comparable device parameters to BHJ OPVs.[19] The nanoparticles were prepared from a wide bandgap semicrystalline conjugated polymer namely poly(2,5-thiophene-alt-5,10-bis(octyloxy)dithieno[3,2-c:3',2'-h][1,5]naphthyridine-5,10-dione) (PTNT)[35] and $PC_{71}BM$ (phenyl C_{71} butyric acid methyl ester). PTNT polymer was chosen in this study as it was demonstrated to perform well in an active layer thickness of up to 400 nm[35], which makes it a relevant polymer for devices fabricated via printing. To gain a better understanding of the influence of the miniemulsion dispersed phase solvent on the nanoparticle properties, PTNT:$PC_{71}BM$ NPs prepared using chloroform as the miniemulsion dispersed phase solvent were also studied. Size distribution, optical, thermomechanical and photovoltaic properties of PTNT:$PC_{71}BM$ nanoparticles prepared using *o*-xylene (NP-xylene) were systematically studied and compared with those processed from chloroform (NP-chloroform). A maximum PCE of 1.65%, with a short circuit current density (J_{SC}) of 4.75 mA/cm^2 was achieved from nanoparticles prepared using *o*-xylene as the miniemulsion dispersed phase solvent as compared to a 1.04% PCE and 2.84 mA/cm^2 of J_{SC} for the dispersions prepared using chloroform as the miniemulsion dispersed phase solvent.

2. Experimental

2.1 PTNT synthesis

Polymer PTNT (Fig. 1) was synthesized by Stille coupling copolymerisation from monomer 2,7-dibromo-5,10-bis(octyloxy)dithieno[3,2-c:3′,2′-h][1,5]naphthyridine-5,10-dione(NT) and 2,5-bis(trimethylstannyl)thiophene as previously reported.[35] The molecular weight was measured by size exclusion chromatography (SEC) in 1,2,4-trichlorobenzene (1,2,4-TCB) at 150 °C. Detailed synthetic procedure and SEC operational conditions are included in Supplementary Information. M_n= 55.7 kg/mol, M_w= 163.2 kg/mol were determined relative to polystyrene standards. Through square wave voltammetry, the HOMO and LUMO energy levels of PTNT are estimated to be -5.9 and -3.6 eV, respectively.[35] Bulk heterojunction (BHJ) solar cells processed using PTNT:$PC_{71}BM$ (1:2 weight ratio) processed from *o*-DCB solution have been reported to achieve a PCE of 5% in a conventional configuration[35] and 5.1% in an inverted structure.[36]

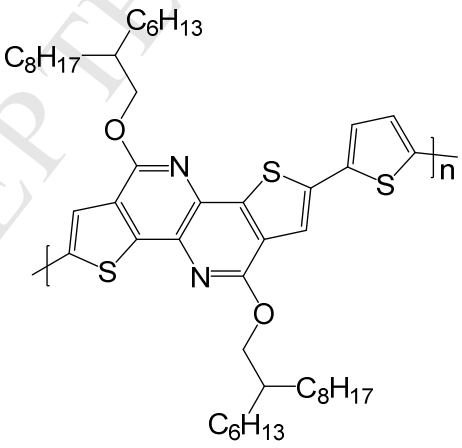

Fig. 1. Chemical structure of PTNT.

2.2 Nanoparticle preparation

$PC_{71}BM$ was purchased from Solenne BV. PTNT:$PC_{71}BM$ nanoparticles were prepared with the weight ratio of 1:2 through the miniemulsion method.[33, 37] The weight ratio was chosen based on the best performance of BHJ devices from a PTNT:$PC_{71}BM$ blend without solvent additive.[35] ~~10 mg of~~ PTNT (10 mg) and ~~20 mg of~~ $PC_{71}BM$ (20 mg) were dissolved in 540 μL of organic solvent (chloroform or *o*-xylene) at 35 °C with stirring at 500 rpm for 2 hours. Meanwhile the aqueous phase was prepared by dissolving ~~33 mg of~~ sodium dodecyl sulphate (SDS) (33 mg) in 2.8 mL of MilliQ water. After ensuring complete dissolution of PTNT and $PC_{71}BM$, the aqueous phase was combined with the organic phase under stirring at 1200 rpm. A macroemulsion was then formed by stirring the mixture at 1200 rpm at 30 °C for approximately 1 hr. To generate the miniemulsion, Vibra-Cell ultrasonic processor VCX 750 with 1/8" stepped probe was introduced to ultra-sonicate the macroemulsion at 30% amplitude for 3 min. Then the miniemulsion was transferred immediately to a heating block and stirred at 1200 rpm to form a stable water dispersion of NPs after complete removal of the residual organic solvent. For nanoparticles prepared using chloroform, the miniemulsion was heated at 60 °C for 3 hr to ensure the complete removal of chloroform whereas in the case of using *o*-xylene, a NPs dispersion was achieved by heating at 75 °C for 6 hr. Additional water was added every hour to compensate for the water loss, which ~~could~~ otherwise results in aggregation of material and precipitation on the wall of the vials. To minimise unwanted SDS from negatively impacting the device performance[27], centrifugal dialysis was introduced to remove excess free surfactant in the dispersion as well as concentrate the active materials in the water dispersion, giving the final dispersion a solids content of 6 wt% in 0.5 mL water.

2.3 Nanoparticle characterization

Scanning electron microscopy (SEM) was performed using an ultra-high resolution field-emission gun scanning electron microscope (Zeiss Merlin) at an accelerating voltage of 2 kV with magnification ranges of 50,000-150,000 X. All SEM samples were spin-coated (3000 rpm for 1 minute) from diluted nanoparticle water dispersion with 1wt% of solids content on conductive silicon substrate. The size distribution of PTNT:$PC_{71}BM$ (1:2 weight ratio) NPs prepared from different organic solvents were characterized from SEM images with a circular Hough transform algorithm.[37-38] In the varied annealing temperature study, all films were pre-dried at 90 °C for 4 min immediately after spin-coating for consistency with device fabrication.

The ultraviolet–visible (UV-vis) study was performed on a Perkin Elmer UV-vis-NIR Lambda950 spectrophotometer. The photoluminescence (PL) measurements were performed on a Varian Cary Eclipse fluorescence spectrophotometer at the excitation wavelength of 450 nm. The PL measurements of NP water dispersions were performed on diluted NP-xylene and NP-chloroform dispersion with the same concentration. Measurements of the solid state were performed on spin coated NP films from original NP dispersion. It should be noted that the study of absorbance change of NP film with and without annealing was measured on the same area on the same film for comparison.

Dynamic mechanical thermal analysis (DMTA) samples were prepared by repeatedly drop-casting the PTNT:$PC_{71}BM$ NP water dispersion onto a 20-30 mm long, approximately 5 mm wide piece of glass fiber mesh, as described elsewhere[39], followed by drying under ambient condition until a uniformly fully covered film on the glass mesh was obtained. The samples were stored in a desiccator overnight to remove most of the water before performing DMTA measurements. DMTA measurements were carried out on a TA Q800 DMA in strain-

controlled mode at a frequency of 1 Hz and an amplitude of 5 µm. The samples were measured under a continuous flow of nitrogen gas with a heating rate of 3 °C per minute. The first run was performed from room temperature up to 80 °C for further drying the sample, followed by a second run from -110 °C to 200 °C. The data from the second run was utilized to study thermomechanical properties of materials in this study.

2.4 Device fabrication

Inverted solar cells with the structure ITO/ZnO/NPs/MoO_3/Ag were fabricated using water dispersed NPs to coat the active layer. Patterned ITO-coated glass substrates (10 Ω/sq, purchased from Xin Yan Technology Ltd) were cleaned using the procedure described elsewhere.[36] ITO-coated glass substrates were first cleaned by soaking in a 5% detergent solution (pyroneg from Johnson Diversey) at 90 °C for 20 minute and then rinsing in deionized (DI) water, before sonicating in DI water, acetone and isopropanol for 10 min each. Substrates were then cleaned in UV-ozone for 20 minute immediately before spin coating the ZnO layer. ZnO sol-gel[40] on the cleaned ITO substrate was heated at 280 °C for 10 minute in air to yield a 25 nm thick film. The PTNT:$PC_{71}BM$ (1:2 weight ratio) NP dispersion was filtered through a PTFE membrane syringe filter (pore size of 0.45 µm) prior to spin coating, and resulted in approximate film thickness of 190 nm. The NP films on ZnO/ITO glass substrates were then dried at 90 °C for 4 minute in air, before transferring to the glove box. It should be noted that 4 minute thermal annealing at 90 °C did not induce NPs sintering (see Fig. S1), further supporting the first run of DMTA scan did not alter the NP structure. The NP films were thermally annealed at 160 °C for 4 minute inside the glove box with nitrogen atmosphere before a thin layer of MoO_3 (12 nm) was thermally evaporated on top of the active layer to serve as a hole transporting layer. Finally the Ag electrode (80 nm) was deposited by thermally evaporating through a shadow mask, which defined the active area to be 0.1 cm^2. To achieve best performing devices, NP solar cells were post-annealed (after the

electrode deposition) for 4 minute in the glove box at 140 °C or 160 °C (as specified in the discussion).

2.5 J-V characterization

I-V properties of solar cells were measured in air by an Oriel solar simulator fitted with a 150 W xenon lamp (Newport), filtered to give an irradiation of 100 mW/cm^2 at AM1.5 and calibrated using a silicon reference cell with NIST traceable certification. The photocurrent–voltage (*I-V*) characteristics of devices were measured through a Keithley 2400 source meter unit. External quantum efficiency (EQE) measurements were performed by a Cornerstone 260™ motorized 1/4 m monochromator (model 74125, Newport) and TracQ basic software for data acquisition.

3. Results and discussion

3.1 Property of nanoparticles

~~PTNT:PC$_{71}$BM (1:2 weight ratio) NPs were prepared using the miniemulsion method[24] with chloroform or *o*-xylene as a miniemulsion dispersed phase solvent. To achieve stable aqueous NP dispersions, chloroform (utilized to form the miniemulsion) was completely removed after heating at 60 °C for 3 hr and *o*-xylene was evaporated by heating at 75 °C for 6 hr, respectively.~~ To evaluate the size of prepared NPs, SEM measurement was performed on NPs in the solid state. SEM images presented in Fig. 2a and b depict the PTNT:PC$_{71}$BM nanoparticulate films for NPs ~~spun~~ prepared from chloroform and *o*-xylene, respectively. NPs were as spun ~~(no thermal treatment)~~ from water-based colloidal dispersions without further treatment. The particulate shape of PTNT:PC$_{71}$BM NPs was found not to be completely spherical, which is typical for NPs made of semicrystalline polymer.[25, 27, 41-43] The size distribution of NPs (Fig. 2c) was measured by applying a circular Hough transform algorithm

to the SEM images of NP films. Since the circular Hough transform algorithm is based on circle calculation, the model resulted in several mismatches (see Fig. S2). Nevertheless the mean diameter of PTNT:$PC_{71}BM$ NPs prepared using chloroform (NP-chloroform) was calculated to be 32 ± 12 nm whereas the nanoparticles from the *o*-xylene batch (NP-xylene) had a mean diameter of 27 ± 11 nm in the solid state. Compared to NP-chloroform, NP-xylene resulted in a slightly narrower size distribution with the presence of fewer large sized NPs on the surface. This observation indicates that the higher temperature and the longer time required to convert the NP-xylene miniemulsion to an aqueous dispersion does not result in material aggregation or further increase in the particle size.

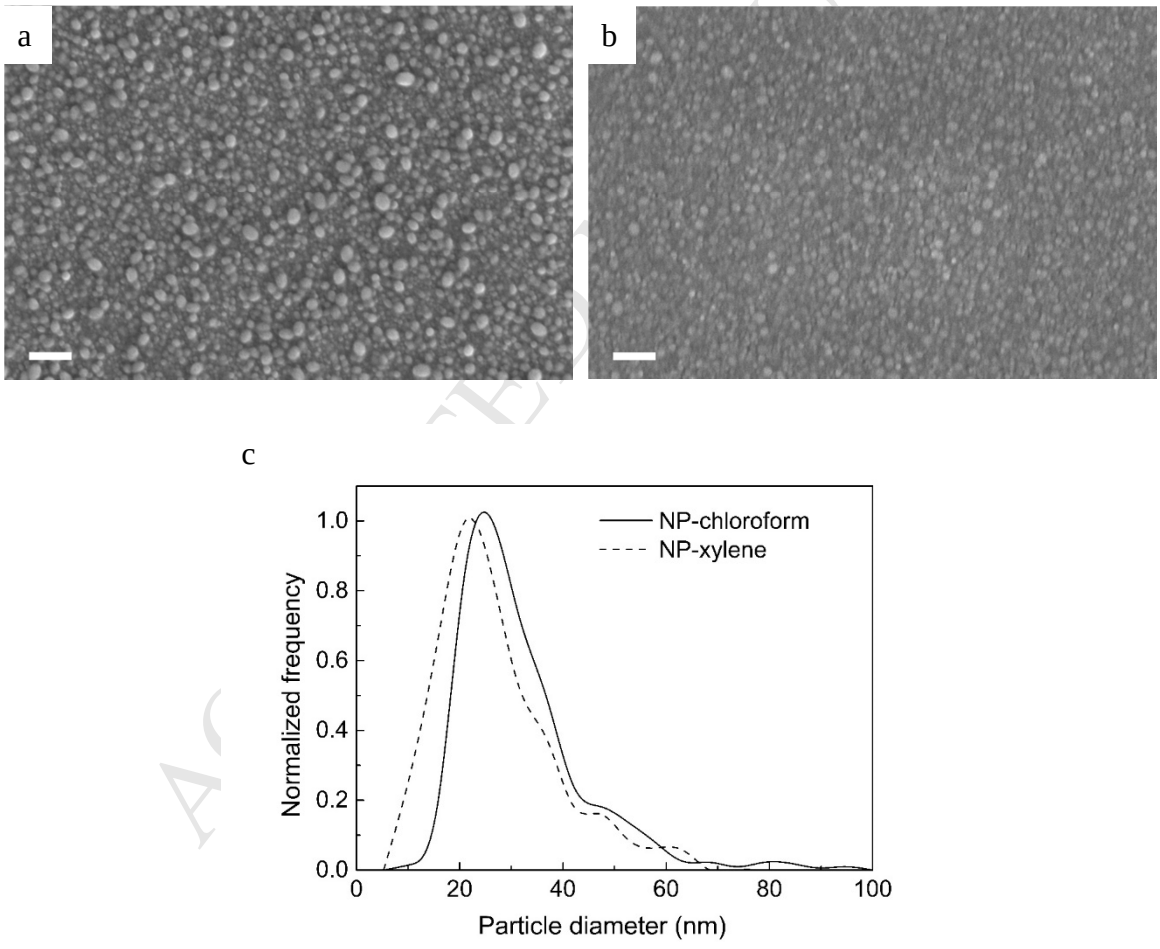

Fig. 2. SEM image of (a) NP-chloroform and (b) NP-xylene. Size distribution of NP-chloroform and NP-xylene (c). Scale bars are 200 nm.

To achieve well performing solar devices using water dispersed NPs, it is imperative to achieve good morphology of the active layer.[44-45] Due to the particulate shape and the core-shell structure of NPs prepared through miniemulsion method[25, 37], the coalescing of NPs could ideally tune the morphology of the active layer and is thus desirable for better charge transport and extraction.[21, 46] To coalesce NPs without inducing defects in the film, thermal-annealing was introduced, which is widely applied to both NP and BHJ solar devices to improve the morphology of the active layer, therefore enhancing the performance of devices.[46-48] The schematic shown in Fig. 3 depicts coalescence of NPs upon annealing in the solid state. SEM and atomic force microscopy (AFM) (see SI varied annealing temperature study) was thus used to systematically study the changes induced in the surface topography of the NP films as a function of annealing temperatures, and to find the ideal annealing temperature which resulted in best performing devices.

Fig. 3. Schematic of NP coalescing upon thermal annealing to form continuous film.

The as spun film prepared from NP-chloroform (Fig. 2a) shows that the separate NPs are clearly distinguishable. The near-edge X-ray absorption fine structure (NEXAFS) spectroscopy measurements (Fig. S3) and scanning transmission X-ray microscopy (STXM) results (Fig. S4) reveal the core-shell structure of PTNT:$PC_{71}BM$ NPs without thermal annealing. Thermal annealing of NP-chloroform films at 100 °C (see Fig. S5a) or 120 °C (Fig. 4a) was not found to make any significant changes on the surface features of the films, as a large degree of nanoparticulate structure was still observed by SEM. The particles were found to interconnect with each other (sinter) after the NP-chloroform film was annealed at 140 °C

(Fig.4b), with some residual nanoparticles presented on the surface. When thermally annealed at 160 °C (Fig. 4c), NPs were sintered and the relatively homogenous film was obtained, which could improve the charge transport[43] and reduce the possibility of charge recombination in the coalesced NP active layer in OPVs.[21] Upon annealing at 180 °C, large aggregates in the NP-chloroform film were observed (Fig. 4d), which was attributed to the crystallization of $PC_{71}BM$.[49] The gross phase separation deteriorated the NP film morphology, which is detrimental for the device performance of NP solar devices.[33, 43, 50] Thus, precise control over the thermal annealing temperature is crucial to achieve a homogenous active layer in OPVs as well as removing the moisture and avoiding large phase separation.[37] Similar behaviour was also found in the case of NP-xylene films, when annealed at different temperatures (Fig. 4e-h). Compared to the reported P3HT:PCBM NPs[51], which require lower annealing temperature to form coalescent film, the slightly harsh annealing performed to sinter PTNT:$PC_{71}BM$ NPs could be explained by the difference in the thermal properties of the polymers used to form NPs as P3HT is reported to have a glass transition temperature (T_g) of 38 °C[39].

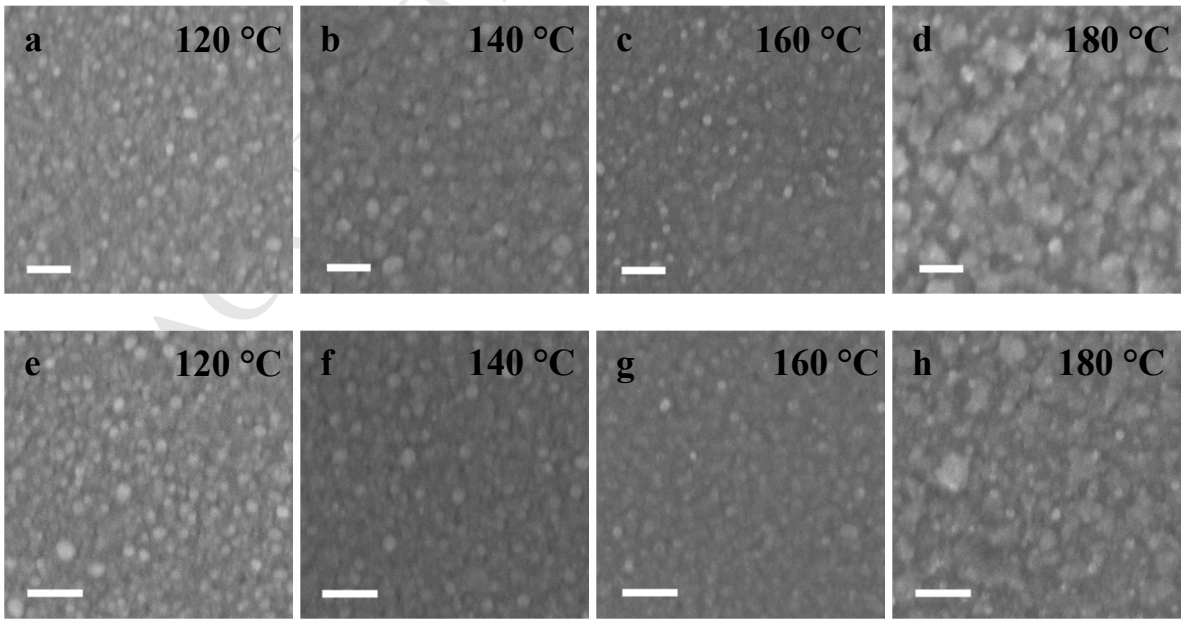

Fig. 4. SEM images of PTNT:$PC_{71}BM$ (1:2) NP films cast from NP-chloroform (a-d) and NP-xylene (e-h) thermally annealed at varied temperature for 4 min. Scale bars are 200 nm.

To further probe the morphological changes and thermomechanical behaviour of PTNT:$PC_{71}BM$ NP films, DMTA measurements [39] were performed on thin films cast from NP-xylene ~~(Fig. 5) and NP-chloroform (see Fig. S6a) as well as pure PTNT (Fig. S6b)~~ and NP-chloroform as well as pure PTNT (Fig. 5). Since DMTA measures the thermal properties of materials with high sensitivity[39, 52-53], it further compliments the SEM study which only probes the surface topography. Fig. 5a shows the storage modulus (*E'*) in the DMTA scan of the NP-xylene sample. ~~The storage modulus (*E'*)~~ was found to drop around 100 °C with a significant loss at 160 ˚C, indicating the softening of the amorphous part of the PTNT-rich phase.[54] Based on the STXM results (Fig. S4), it is known that the nanoparticles have a core-shell structure with a PTNT-rich NP shell and a $PC_{71}BM$-rich NP core. As such, the nanoparticles should start to coalesce only when PTNT in the polymer-rich shell reaches the rubbery state[55] similarly to P3HT:PCBM NPs[25]. Thus, the significant drop in the *E'* observed using DMTA agrees well with the coalescence of the nanoparticles in thin films observed using SEM. Beyond 160 ˚C, the stiffness (*E'*) of the DMTA sample was again found to increase, which is attributed to the crystallization of $PC_{71}BM$ in the $PC_{71}BM$-rich phase after the coalescence of the NPs, revealing the maximum temperature before detrimental crystallization occurs. This behaviour was also observed in SEM as drastic phase separation and coarsening of the film (Fig. 4h). ~~The DMTA temperature scan of the NPs prepared using chloroform can be found in the Supplementary Information Fig. S6a and they show a similar thermomechanical behaviour, whereas the PTNT DMTA scan (Fig. S6b) doesn't show the increase of *E'* above 160 °C.~~ The DMTA temperature scan of the NPs prepared using chloroform (Fig. 5b) shows a similar thermomechanical behaviour, whereas the neat PTNT DMTA scan (Fig. 5c) did not show the increase of *E'* above 160 °C, which further confirms

the increase in stiffness being attributed to the $PC_{71}BM$ thermal transition. Since PTNT is a conjugated polymer with large side chains and more rigid backbones than P3HT, the onset of the decrease in storage modules at −40 °C is attributed to the relaxation of the side chains, i.e. β transition. The higher β transition temperature (T_β) of PTNT compared to the T_β P3HT[39, 56] also indicates higher T_g of PTNT, which further supports the higher temperature required to coalesce PTNT:$PC_{71}BM$ NPs compared to the P3HT:PCBM NPs[51].

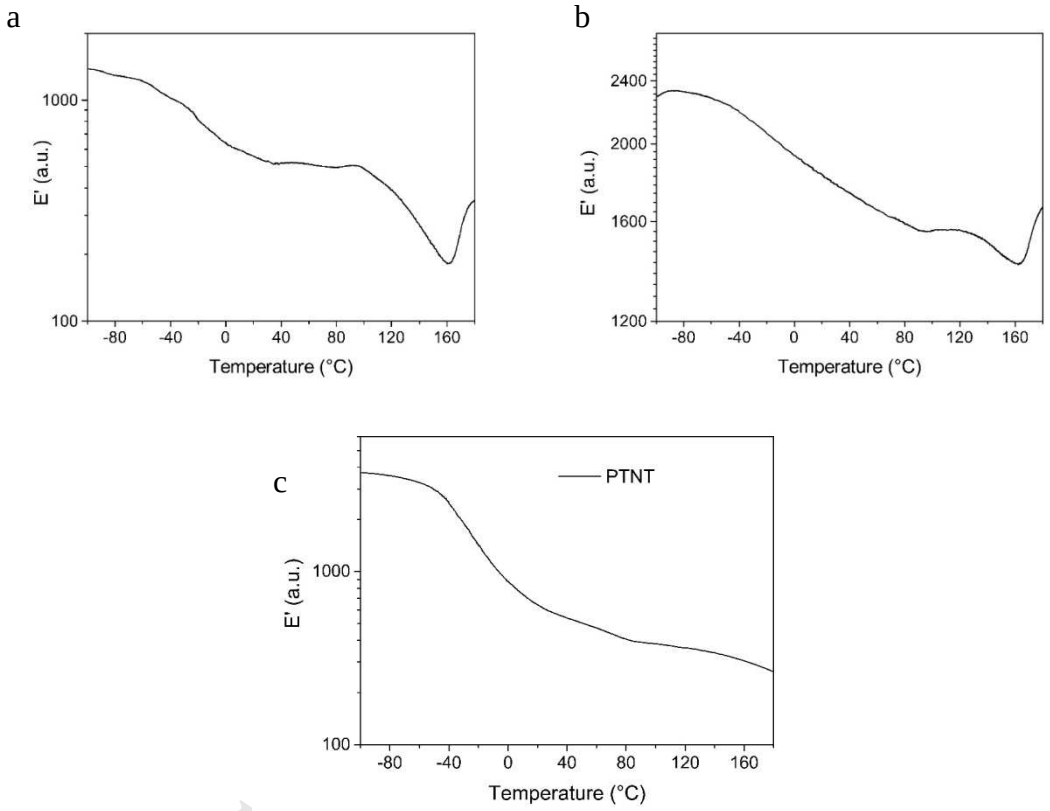

Fig. 5. Storage modulus (*E'*) as a function of temperature in a DMTA temperature scan of (a) NP-xylene, (b) NP-chloroform and (c) neat PTNT supported by a glass fiber mesh.

3.2 ~~3.1~~ Optical properties of nanoparticles

To probe the optical properties of NPs prepared using different solvents, UV-vis and photoluminescence (PL) measurements were carried out on NP films as well as NP dispersions. Fig. 6 shows the UV-vis absorption spectra of solid state films and PL spectra

from both batches of NPs. The broad absorption band beyond 400 nm is attributed to the intramolecular charge transfer between donor and acceptor segments in the PTNT polymer backbones.[35] The absorption peak below 400 nm is primarily attributed to the absorbance of $PC_{71}BM$, while the vibronic peaks at 522 nm in the absorption spectra are attributed to the π-π stacking of polymer backbone[35] (Fig. S6a). It can be observed that after thermal annealing the absorbance of PTNT:$PC_{71}BM$ NP film was increased (Fig. 6a,b**).** The increased absorption upon annealing could be due to the increased crystallinity and enhanced ordering of PTNT in the annealed films[22, 57], which was also observed in annealed PTNT:$PC_{71}BM$ BHJ films (presented in Fig. S6b and c). The thermal annealing at 160 °C for 4 min did not lead to blue-shifted onset or decrease of the light absorbance of the PTNT:$PC_{71}BM$ NP films, revealing no thermal degradation of materials in the NP film during short-term thermal annealing.

The PL spectra shown in Fig. 6c compare the quenching of PL signal in NP-chloroform and NP-xylene water dispersion. A higher PL intensity is observed for the NP-xylene dispersion (Fig. 6c), which was attributed to a higher degree of donor-acceptor material phase separation within the NPs[22, 50, 58], suggesting that larger and/or purer polymer domains already existed post NP preparation. Similar to the result found in the PL of the aqueous dispersions, NP-xylene film as spun (Fig. 6d) also shows lower PL quenching in the emission band of PTNT compared to NP-chloroform film as spun, indicating the difference in nanomorphology of the NPs prepared from different solvents. However, upon thermal annealing a lower PL signal was found in NP-xylene film compared to the annealed NP-chloroform film, indicating a finer intermixed morphology was achieved. The increase in PL intensity of NP films after annealing (Fig. 6d) indicates an increase in crystallinity of polymer domains or a higher degree of phase separation, generated by $PC_{71}BM$ diffusion from amorphous PTNT-rich domains, resulting in lower PL quenching of PTNT emission upon annealing.[33, 59] It must be

noted that compared to the PL of PTNT pristine film, annealed NP film shows high degree of quenched PL signal (Fig. S6d), indicating efficient photo-induced charge transfer between PTNT and $PC_{71}BM$.[60]

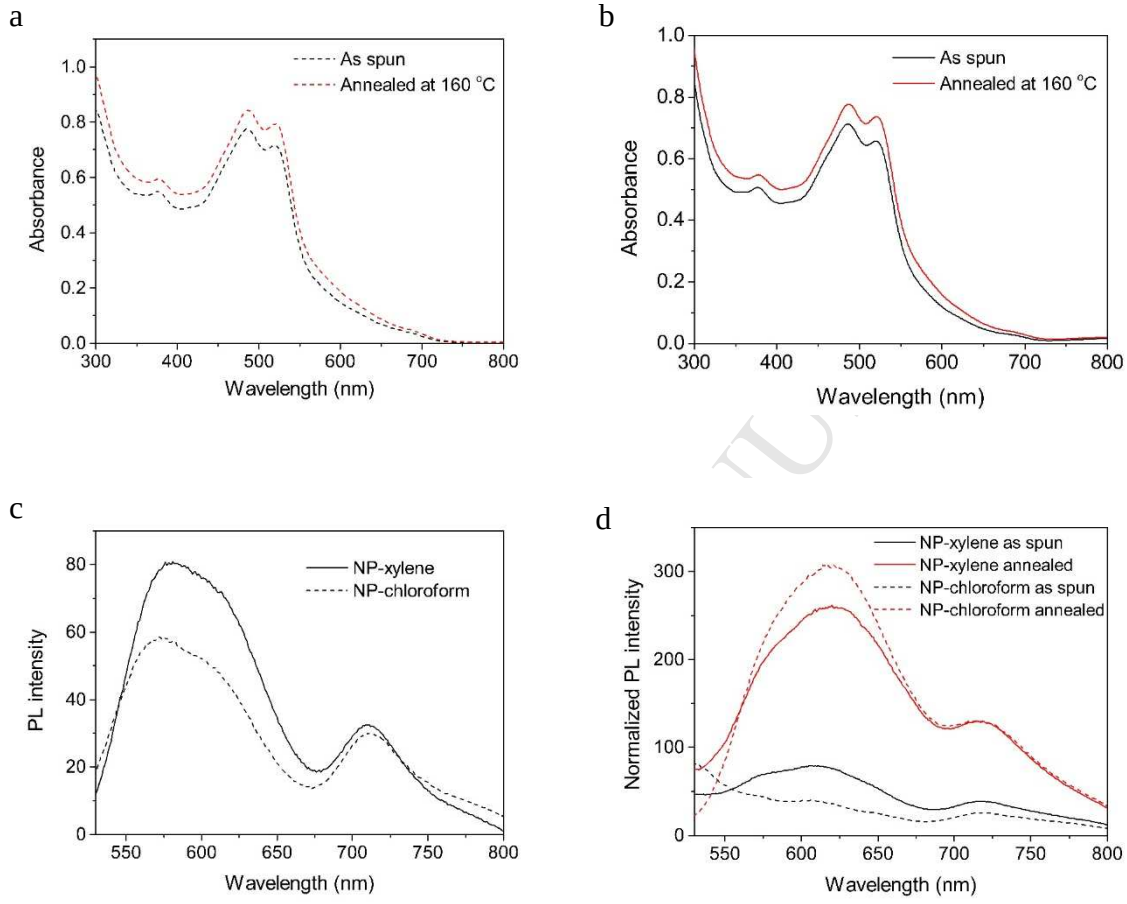

Fig. 6. UV-vis absorption spectra of PTNT:$PC_{71}BM$ NP-chloroform film (a) and NP-xylene film (b) as spun and thermally annealed at 160 °C for 4 min. PL spectra of (c) NP-xylene and NP-chloroform dispersions and (d) NP-xylene and NP-chloroform films as spun and annealed at 160 °C.

3.3 ~~3.2~~ Photovoltaic characterizations

In order to test the photovoltaic properties of NPs, solar cells were fabricated and tested with the active layer spin-coated from NP dispersion (presented in Fig. S7) followed by annealing at different temperatures. The device performance was found to be strongly dependant on the

annealing temperature of the NP films (see Fig. S8, Table S2), with best performing devices being the ones sintered at 160 °C which is in good agreement with the observations made in the morphological studies with SEM and DMTA.

The device characteristics of solar cells fabricated with NP-chloroform and NP-xylene films annealed at 160 °C are listed in Table 1. NP-chloroform films after thermal annealing at 160 °C were found to result in solar cells with a maximum PCE of 0.76%, a J_{SC} of 2.60 mA/cm^2 and fill factor (*FF*) of 32%. The PCE of these devices was further increased up to 1.04% accompanied by slight increase in J_{SC} to 2.84 mA/cm^2 and a significant increase in *FF* to 43% upon post-annealing the complete devices at 160 °C. Thermal treatment after the deposition of electrode is known to enhance the performance of NP based solar cells.[37, 61] Although post-annealing at 160 °C resulted in a slightly higher PCE of 1.04% as compared to the PCE of 0.98% when post-annealed at 140 °C, the standard deviation in the device characteristics in the case of devices post-annealed at 160 °C was higher than that at 140 °C. The increase in the standard deviation could be a result of the uneven distribution of gross phase separation happening during post-annealing at high temperature. The representative *J-V* curves of NP-chloroform based devices with and without post-annealing are shown in Fig. 7a. It must be noted that the open circuit voltage (V_{OC}) of these devices was found to be as high as 0.90 V, which is comparable to their BHJ counterparts processed from organic solvents (see Table S3).[35-36] This suggests that the performance of PTNT:$PC_{71}BM$ NP solar cells is mainly limited by the lower current and lower *FF*, both of which can be highly dependent on the NP film morphology and the nature of the donor/acceptor interface.[27] Furthermore, compared to solution-processed BHJ solar cells[35], the lower performance of NP devices could be explained by the relatively isolated polymer and $PC_{71}BM$ domains with insufficient connection of fullerene-rich core, which impedes the charge separation[62] as well as increasing the possibility of non-geminate recombination[63].

OPVs fabricated from NP-xylene films thermally annealed at 160 °C were found to have higher J_{SC} of 3.91 mA/cm^2 and comparable V_{OC} of 0.88 V, resulting in a PCE of 1.3%. Post-annealing at 140 °C after the deposition of electrode further increased the PCE up to 1.65 % with the highest J_{SC} of 4.73 mA/cm^2, 0.89 V in V_{OC} and 39 % in *FF*. Clearly, the higher performance of the NP-xylene based devices as compared to the NP-chloroform devices is largely due to the higher current in these devices, which is indicative of a relatively more favourable donor-acceptor morphology of NP-xylene film after thermal annealing and is consistent with the observation in the PL measurement. The representative *J-V* curves of NP-xylene based devices are presented in Fig. 7b. External quantum efficiency (EQE) of NP device post-annealed at 140 °C was found to increase in both PTNT and $PC_{71}BM$ photon absorption range as compared to the non post-annealed devices (Fig. 7c). This could possibly be explained due to better exciton dissociation or reduced charge recombination resulted from the phase separation between polymer and $PC_{71}BM$.[64] When a higher post-annealing temperature (i.e. 160 °C) was applied to the device, a decline in the mean value of J_{SC} was observed as well as V_{OC} compared to the device performance without post-annealing. However, an improvement in *FF* compensated the decrease in J_{SC} and V_{OC}, and resulted in slightly improved efficiency, which is 1.33% on average, compared to the values in device without post-annealing. The EQE of NP-xylene based device post-annealed at 160 °C showed the contribution of photon harvesting property in $PC_{71}BM$ region (below 400 nm) was increased compared to the contribution from PTNT region (above 400 nm), which can be revealed from the decline of EQE between 450 nm to 600 nm photon wavelength (Fig. 7c). Considering 160 °C is approaching the crystallisation temperature of $PC_{71}BM$[49], the increase in EQE in the wavelength below 400 nm could be attributed to the crystallization appearing in the pure $PC_{71}BM$ domains, which also agrees with the storage modulus increasing beyond 160 °C (Fig. 5).

Either with or without post-annealing, the NP solar devices fabricated from *o*-xylene batch PTNT:$PC_{71}BM$ (1:2 weight ratio) NPs achieved higher J_{SC} and efficiency compared to the NP devices produced from NP-chloroform. However, there is no significant difference in *FF* and V_{OC} between different batches of NPs as long as they were thermally treated in the same way. The increase in J_{SC} is attributed to a finer intermixed nanomorphology in annealed NP-xylene film, which is also suggested by the PL of annealed NP films. The difference in the morphology of NP active layer indicates that post-preparation of NPs, the internal morphology of NPs was changed by altering the miniemulsion dispersed phase solvent from chloroform to *o*-xylene. The difference of the internal morphology between NP-xylene and NP-chloroform was revealed from the varied PL intensity observed in different batches of NP dispersions.

BHJ solar cells were also fabricated from PTNT:$PC_{71}BM$ (1:2 weight ratio) blends using chloroform and *o*-xylene as the processing solvents, with the same device geometry. The BHJ devices gave highest PCE of 1.20% with chloroform and 0.84% using *o*-xylene (see Table S3), due to the unfavourable film quality induced by the processing solvents. The NP-OPVs based on aqueous NP-xylene achieved comparable photovoltaic performance without using any harmful solvent during the device fabrication, though the efficiency of PTNT:$PC_{71}BM$ BHJ devices could be improved by altering the processing solvent and using additives[35-36].

Table 1 PTNT:$PC_{71}BM$ (1:2 weight ratio) NP device characteristics of best devices for varied post-annealing condition, with average ± standard deviations over 8 devices in parentheses. (All the NP films were thermally annealed at 160 °C before the deposition of electrode.)

Active layer	**Annealing condition**	**J_{SC} (mA/cm^2)**	**FF (%)**	**V_{OC} (V)**	**PCE (%)**

NP-chloroform	No post-annealing	2.60 (2.48 ± 0.10)	32 (33 ± 2)	0.90 (0.88 ± 0.03)	0.76 (0.73 ± 0.01)
	140 °C post-annealing	2.75 (2.72 ± 0.10)	39 (39 ± 1)	0.90 (0.88 ± 0.01)	0.98 (0.94 ± 0.02)
	160 °C post-annealing	2.84 (2.59 ± 0.23)	43 (42 ± 1)	0.86 (0.86 ± 0.02)	1.04 (0.93 ± 0.09)
NP-xylene	No post-annealing	4.00 (3.91 ± 0.13)	36 (36 ± 1)	0.89 (0.88 ± 0.02)	1.30 (1.24 ± 0.05)
	140 °C post-annealing	4.73 (4.58 ± 0.13)	39 (39 ± 1)	0.89 (0.87 ± 0.02)	1.65 (1.56 ± 0.06)
	160 °C post-annealing	4.15 (3.76 ± 0.22)	42 (42 ± 1)	0.86 (0.84 ± 0.02)	1.51 (1.33 ± 0.10)

a

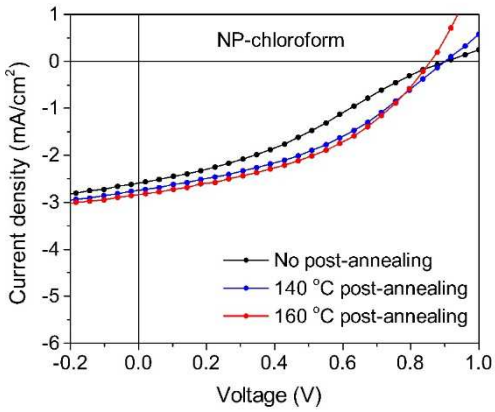

b

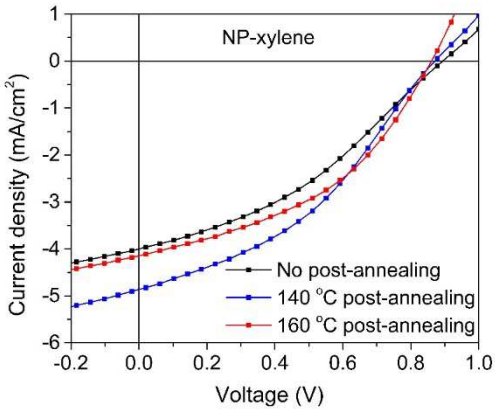

c

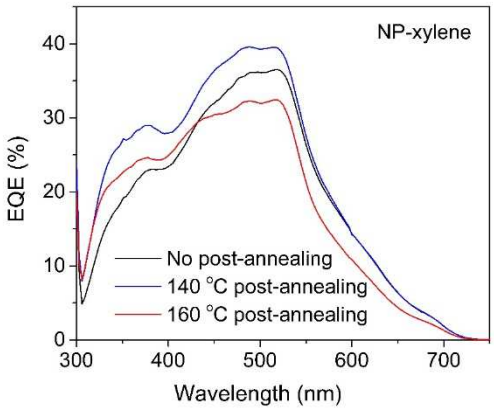

Fig. 7. Representative J-V curves of devices based on (a) NP-chloroform and (b) NP-xylene without post-annealing and post-annealed at different temperatures. (c) EQE of NP-xylene devices without post-annealing and post-annealed at different temperatures.

4. Conclusions

Water-dispersed NPs have been prepared from the conjugated polymer PTNT for the first time and non-chlorinated solvent, *o*-xylene, has been used in the miniemulsion method to prepare photoactive NPs for the first time in the NP-OPV research. The NP solar devices fabricated from aqueous PTNT:$PC_{71}BM$ nanoparticles using *o*-xylene as the miniemulsion dispersed phase solvent achieved higher PCE of 1.65%, after optimal thermal-annealing conditions were applied to both the NP layer and the complete device, compared to the chloroform batch counterparts. By introducing *o*-xylene as the miniemulsion dispersed phase solvent to prepare nanoparticles, a water dispersion minimized the amount of organic solvent required in device fabrication and eliminated the utilization of harmful chlorinated solvents in the solar cell ink preparation. The study of PTNT:$PC_{71}BM$ NPs can potentially be beneficial for the up-scaling of OPV fabrication in future. Furthermore, the preparation procedure presented opens the possibility of using other environment-friendly solvents to achieve aqueous NPs for OPVs.

Acknowledgements

The authors thank the Flinders University and the South Australian government for financial support. This research was supported by the Australian Research Council's Discovery Projects funding scheme (Project DP170102467). The device fabrication facilities including the glove box and thermal evaporator at Flinders University are supported by the Australian Nano Fabrication Facility (ANFF) and the Australian Microscopy and Microanalysis

Research Facility (AMMRF), which are gratefully acknowledged. Special thanks to the University of Newcastle Electron Microscopy and X-ray Unit. This work was performed in part at the Materials node of the Australian National Fabrication Facility, which is a company established under the National Collaborative Research Infrastructure Strategy to provide nano- and microfabrication facilities for Australia's researchers. The ALS is supported by the Director, Office of Science, Office of Basic Energy Sciences, of the U.S. Department of Energy under Contract No. DE-AC02-05CH11231.

References

1. Nejat, P.; Jomehzadeh, F.; Taheri, M. M.; Gohari, M.; Abd. Majid, M. Z., A global review of energy consumption, CO2 emissions and policy in the residential sector (with an overview of the top ten CO2 emitting countries). *Renewable and Sustainable Energy Reviews* **2015,** *43*, 843-862.
2. Luderer, G.; Krey, V.; Calvin, K.; Merrick, J.; Mima, S.; Pietzcker, R.; Van Vliet, J.; Wada, K., The role of renewable energy in climate stabilization: results from the EMF27 scenarios. *Climatic Change* **2014,** *123* (3-4), 427-441.
3. Eisenberg, R.; Nocera, D. G., Preface: Overview of the forum on solar and renewable energy. *Inorganic chemistry* **2005,** *44* (20), 6799-6801.
4. Li, S.; Lei, M.; Lv, M.; Watkins, S. E.; Tan, Z. a.; Zhu, J.; Hou, J.; Chen, X.; Li, Y., [6,6]-Phenyl-C61-Butyric Acid Dimethylamino Ester as a Cathode Buffer Layer for High-Performance Polymer Solar Cells. *Advanced Energy Materials* **2013,** *3* (12), 1569-1574.
5. Kalogirou, S. A., *Solar energy engineering: processes and systems*. Academic Press: 2013.
6. Xiao, B.; Wu, H.; Cao, Y., Solution-processed cathode interfacial layer materials for high-efficiency polymer solar cells. *Materials Today* **2015**.
7. Burgués-Ceballos, I.; Machui, F.; Min, J.; Ameri, T.; Voigt, M. M.; Luponosov, Y. N.; Ponomarenko, S. A.; Lacharmoise, P. D.; Campoy-Quiles, M.; Brabec, C. J., Solubility Based Identification of Green Solvents for Small Molecule Organic Solar Cells. *Advanced Functional Materials* **2014,** *24* (10), 1449-1457.
8. Angmo, D.; Larsen-Olsen, T. T.; Jørgensen, M.; Søndergaard, R. R.; Krebs, F. C., Roll-to-Roll Inkjet Printing and Photonic Sintering of Electrodes for ITO Free Polymer Solar Cell Modules and Facile Product Integration. *Advanced Energy Materials* **2013,** *3* (2), 172-175.
9. Noh, J.; Jeong, S.; Lee, J. Y., Ultrafast formation of air-processable and high-quality polymer films on an aqueous substrate. *Nat Commun* **2016,** *7*, 12374.
10. Zhao, W.; Li, S.; Yao, H.; Zhang, S.; Zhang, Y.; Yang, B.; Hou, J., Molecular Optimization Enables over 13% Efficiency in Organic Solar Cells. *J Am Chem Soc* **2017,** *139* (21), 7148-7151.
11. Gedefaw, D.; Sharma, A.; Pan, X.; Bjuggren, J. M.; Kroon, R.; Gregoriou, V. G.; Chochos, C. L.; Andersson, M. R., Optimization of the power conversion efficiency in high

bandgap pyridopyridinedithiophene-based conjugated polymers for organic photovoltaics by the random terpolymer approach. *European Polymer Journal* **2017,** *91*, 92-99.
12. Stapleton, A.; Vaughan, B.; Xue, B.; Sesa, E.; Burke, K.; Zhou, X.; Bryant, G.; Werzer, O.; Nelson, A.; David Kilcoyne, A. L.; Thomsen, L.; Wanless, E.; Belcher, W.; Dastoor, P., A multilayered approach to polyfluorene water-based organic photovoltaics. *Solar Energy Materials and Solar Cells* **2012,** *102*, 114-124.
13. Andersen, T. R.; Larsen-Olsen, T. T.; Andreasen, B.; Bottiger, A. P.; Carle, J. E.; Helgesen, M.; Bundgaard, E.; Norrman, K.; Andreasen, J. W.; Jørgensen, M., Aqueous processing of low-band-gap polymer solar cells using roll-to-roll methods. *ACS nano* **2011,** *5* (5), 4188-4196.
14. Krebs, F. C., Fabrication and processing of polymer solar cells: A review of printing and coating techniques. *Solar Energy Materials and Solar Cells* **2009,** *93* (4), 394-412.
15. Krebs, F. C.; Tromholt, T.; Jorgensen, M., Upscaling of polymer solar cell fabrication using full roll-to-roll processing. *Nanoscale* **2010,** *2* (6), 873-86.
16. Brautbar, N.; Williams, J., 2nd, Industrial solvents and liver toxicity: risk assessment, risk factors and mechanisms. *Int J Hyg Environ Health* **2002,** *205* (6), 479-91.
17. Moran, M. J.; Zogorski, J. S.; Squillace, P. J., Chlorinated Solvents in Groundwater of the United States. *Environmental Science & Technology* **2007,** *41* (1), 74-81.
18. Chen, X.; Liu, X.; Burgers, M. A.; Huang, Y.; Bazan, G. C., Green-solvent-processed molecular solar cells. *Angew Chem Int Ed Engl* **2014,** *53* (52), 14378-81.
19. Zhang, S.; Ye, L.; Zhang, H.; Hou, J., Green-solvent-processable organic solar cells. *Materials Today* **2016,** *19* (9), 533-543.
20. Fan, B.; Ying, L.; Wang, Z.; He, B.; Jiang, X.-F.; Huang, F.; Cao, Y., Optimisation of processing solvent and molecular weight for the production of green-solvent-processed all-polymer solar cells with a power conversion efficiency over 9%. *Energy Environ. Sci.* **2017,** *10* (5), 1243-1251.
21. Schwarz, K. N.; Farley, S. B.; Smith, T. A.; Ghiggino, K. P., Charge generation and morphology in P3HT:PCBM nanoparticles prepared by mini-emulsion and reprecipitation methods. *Nanoscale* **2015,** *7* (47), 19899-904.
22. Darwis, D.; Holmes, N.; Elkington, D.; David Kilcoyne, A. L.; Bryant, G.; Zhou, X.; Dastoor, P.; Belcher, W., Surfactant-free nanoparticulate organic photovoltaics. *Solar Energy Materials and Solar Cells* **2014,** *121*, 99-107.
23. Gärtner, S.; Christmann, M.; Sankaran, S.; Röhm, H.; Prinz, E.-M.; Penth, F.; Pütz, A.; Türeli, A. E.; Penth, B.; Baumstümmler, B.; Colsmann, A., Eco-Friendly Fabrication of 4% Efficient Organic Solar Cells from Surfactant-Free P3HT:ICBA Nanoparticle Dispersions. *Advanced Materials* **2014,** *26* (38), 6653-6657.
24. Landfester, K.; Montenegro, R.; Scherf, U.; GüNTNER, R.; Asawapirom, U.; Patil, S.; Neher, D.; Kietzke, T., Semiconducting polymer nanospheres in aqueous dispersion prepared by a miniemulsion process. *Advanced Materials* **2002,** *14* (9), 651-655.
25. Holmes, N. P.; Burke, K. B.; Sista, P.; Barr, M.; Magurudeniya, H. D.; Stefan, M. C.; Kilcoyne, A. L. D.; Zhou, X.; Dastoor, P. C.; Belcher, W. J., Nano-domain behaviour in P3HT:PCBM nanoparticles, relating material properties to morphological changes. *Solar Energy Materials and Solar Cells* **2013,** *117*, 437-445.
26. D'Olieslaeger, L.; Pfannmöller, M.; Fron, E.; Cardinaletti, I.; Van Der Auweraer, M.; Van Tendeloo, G.; Bals, S.; Maes, W.; Vanderzande, D.; Manca, J.; Ethirajan, A., Tuning of PCDTBT:PC71BM blend nanoparticles for eco-friendly processing of polymer solar cells. *Solar Energy Materials and Solar Cells* **2017,** *159*, 179-188.
27. Colberts, F. J. M.; Wienk, M. M.; Janssen, R. A. J., Aqueous Nanoparticle Polymer Solar Cells: Effects of Surfactant Concentration and Processing on Device Performance. *ACS Appl Mater Interfaces* **2017,** *9* (15), 13380-13389.

28. Parrenin, L.; Laurans, G.; Pavlopoulou, E.; Fleury, G.; Pecastaings, G.; Brochon, C.; Vignau, L.; Hadziioannou, G.; Cloutet, E., Photoactive Donor-Acceptor Composite Nanoparticles Dispersed in Water. *Langmuir* **2017,** *33* (6), 1507-1515.
29. Prunet, G.; Parrenin, L.; Pavlopoulou, E.; Pecastaings, G.; Brochon, C.; Hadziioannou, G.; Cloutet, E., Aqueous PCDTBT:PC71 BM Photovoltaic Inks Made by Nanoprecipitation. *Macromol Rapid Commun* **2017**.
30. Kuehne, A. J.; Gather, M. C.; Sprakel, J., Monodisperse conjugated polymer particles by Suzuki-Miyaura dispersion polymerization. *Nat Commun* **2012,** *3*, 1088.
31. Anwar, N.; Willms, T.; Grimme, B.; Kuehne, A. J. C., Light-Switchable and Monodisperse Conjugated Polymer Particles. *ACS Macro Letters* **2013,** *2* (9), 766-769.
32. Parrenin, L.; Brochon, C.; Hadziioannou, G.; Cloutet, E., Low Bandgap Semiconducting Copolymer Nanoparticles by Suzuki Cross-Coupling Polymerization in Alcoholic Dispersed Media. *Macromol Rapid Commun* **2015,** *36* (20), 1816-21.
33. Ulum, S.; Holmes, N.; Darwis, D.; Burke, K.; David Kilcoyne, A. L.; Zhou, X.; Belcher, W.; Dastoor, P., Determining the structural motif of P3HT:PCBM nanoparticulate organic photovoltaic devices. *Solar Energy Materials and Solar Cells* **2013,** *110*, 43-48.
34. D'Olieslaeger, L.; Pirotte, G.; Cardinaletti, I.; D'Haen, J.; Manca, J.; Vanderzande, D.; Maes, W.; Ethirajan, A., Eco-friendly fabrication of PBDTTPD:PC71BM solar cells reaching a PCE of 3.8% using water-based nanoparticle dispersions. *Organic Electronics* **2017,** *42*, 42-46.
35. Kroon, R.; Diaz de Zerio Mendaza, A.; Himmelberger, S.; Bergqvist, J.; Bäcke, O.; Faria, G. C.; Gao, F.; Obaid, A.; Zhuang, W.; Gedefaw, D.; Olsson, E.; Inganäs, O.; Salleo, A.; Müller, C.; Andersson, M. R., A New Tetracyclic Lactam Building Block for Thick, Broad-Bandgap Photovoltaics. *Journal of the American Chemical Society* **2014,** *136* (33), 11578-11581.
36. Sharma, A.; Kroon, R.; Lewis, D. A.; Andersson, G. G.; Andersson, M. R., Poly(4-vinylpyridine): A New Interface Layer for Organic Solar Cells. *ACS Appl Mater Interfaces* **2017,** *9* (12), 10929-10936.
37. Holmes, N. P.; Marks, M.; Kumar, P.; Kroon, R.; Barr, M. G.; Nicolaidis, N.; Feron, K.; Pivrikas, A.; Fahy, A.; Mendaza, A. D. D. Z.; Kilcoyne, A.; Müller, C.; Zhou, X.; Andersson, M. R.; Dastoor, P. C.; Belcher, W. J., Nano-pathways: Bridging the divide between water-processable nanoparticulate and bulk heterojunction organic photovoltaics. *Nano Energy* **2016,** *19*, 495-510.
38. Wang, Y.; Cheng, G., Application of gradient-based Hough transform to the detection of corrosion pits in optical images. *Applied Surface Science* **2016,** *366*, 9-18.
39. Sharma, A.; Pan, X.; Campbell, J. A.; Andersson, M. R.; Lewis, D. A., Unravelling the Thermomechanical Properties of Bulk Heterojunction Blends in Polymer Solar Cells. *Macromolecules* **2017,** *50* (8), 3347-3354.
40. Sun, Y.; Seo, J. H.; Takacs, C. J.; Seifter, J.; Heeger, A. J., Inverted polymer solar cells integrated with a low-temperature-annealed sol-gel-derived ZnO Film as an electron transport layer. *Adv Mater* **2011,** *23* (14), 1679-83.
41. Hu, Z.; Gesquiere, A. J., PCBM concentration dependent morphology of P3HT in composite P3HT/PCBM nanoparticles. *Chemical Physics Letters* **2009,** *476* (1-3), 51-55.
42. Hu, Z.; Tenery, D.; Bonner, M. S.; Gesquiere, A. J., Correlation between spectroscopic and morphological properties of composite P3HT/PCBM nanoparticles studied by single particle spectroscopy. *Journal of Luminescence* **2010,** *130* (5), 771-780.
43. Vaughan, B.; Williams, E. L.; Holmes, N. P.; Sonar, P.; Dodabalapur, A.; Dastoor, P. C.; Belcher, W. J., Water-based nanoparticulate solar cells using a diketopyrrolopyrrole donor polymer. *Phys Chem Chem Phys* **2014,** *16* (6), 2647-53.

44. Benanti, T.; Venkataraman, D., Organic Solar Cells: An Overview Focusing on Active Layer Morphology. *Photosynth Res* **2006,** *87* (1), 73-81.
45. Treat, N. D.; Chabinyc, M. L., Phase separation in bulk heterojunctions of semiconducting polymers and fullerenes for photovoltaics. *Annu Rev Phys Chem* **2014,** *65*, 59-81.
46. Ulum, S.; Holmes, N.; Barr, M.; Kilcoyne, A. L. D.; Gong, B. B.; Zhou, X.; Belcher, W.; Dastoor, P., The role of miscibility in polymer:fullerene nanoparticulate organic photovoltaic devices. *Nano Energy* **2013,** *2* (5), 897-905.
47. Dam, H. F.; Holmes, N. P.; Andersen, T. R.; Larsen-Olsen, T. T.; Barr, M.; Kilcoyne, A. L. D.; Zhou, X.; Dastoor, P. C.; Krebs, F. C.; Belcher, W. J., The effect of mesomorphology upon the performance of nanoparticulate organic photovoltaic devices. *Solar Energy Materials and Solar Cells* **2015,** *138*, 102-108.
48. Xia, Y.; Musumeci, C.; Bergqvist, J.; Ma, W.; Gao, F.; Tang, Z.; Bai, S.; Jin, Y.; Zhu, C.; Kroon, R.; Wang, C.; Andersson, M. R.; Hou, L.; Inganäs, O.; Wang, E., Inverted all-polymer solar cells based on a quinoxaline–thiophene/naphthalene-diimide polymer blend improved by annealing. *J. Mater. Chem. A* **2016,** *4* (10), 3835-3843.
49. Leman, D.; Kelly, M. A.; Ness, S.; Engmann, S.; Herzing, A.; Snyder, C.; Ro, H. W.; Kline, R. J.; DeLongchamp, D. M.; Richter, L. J., In Situ Characterization of Polymer–Fullerene Bilayer Stability. *Macromolecules* **2015,** *48* (2), 383-392.
50. Holmes, N. P.; Ulum, S.; Sista, P.; Burke, K. B.; Wilson, M. G.; Stefan, M. C.; Zhou, X.; Dastoor, P. C.; Belcher, W. J., The effect of polymer molecular weight on P3HT:PCBM nanoparticulate organic photovoltaic device performance. *Solar Energy Materials and Solar Cells* **2014,** *128*, 369-377.
51. Pedersen, E. B. L.; Pedersen, M. C.; Simonsen, S. B.; Brandt, R. G.; Böttiger, A. P. L.; Andersen, T. R.; Jiang, W.; Xie, Z. Y.; Krebs, F. C.; Arleth, L.; Andreasen, J. W., Structure and crystallinity of water dispersible photoactive nanoparticles for organic solar cells. *J. Mater. Chem. A* **2015,** *3* (33), 17022-17031.
52. Li, D.; Brisson, J., DMTA and FTIR Investigation of the Phase Behavior of Poly(methyl methacrylate)−Poly(4-vinylphenol) Blends. *Macromolecules* **1996,** *29* (3), 868-874.
53. Goertzen, W. K.; Kessler, M. R., Dynamic mechanical analysis of carbon/epoxy composites for structural pipeline repair. *Composites Part B: Engineering* **2007,** *38* (1), 1-9.
54. Matsuoka, S., *Relaxation phenomena in polymers*. Hanser Munich etc.: 1992.
55. Karagiannidis, P. G.; Stergiou, A. C.; Karayannidis, G. P., Study of crystallinity and thermomechanical analysis of annealed poly(ethylene terephthalate) films. *European Polymer Journal* **2008,** *44* (5), 1475-1486.
56. Kuila, B. K.; Nandi, A. K., Structural Hierarchy in Melt-Processed Poly(3-hexyl thiophene)−Montmorillonite Clay Nanocomposites: Novel Physical, Mechanical, Optical, and Conductivity Properties. *The Journal of Physical Chemistry B* **2006,** *110* (4), 1621-1631.
57. Kim, K.; Liu, J.; Namboothiry, M. A. G.; Carroll, D. L., Roles of donor and acceptor nanodomains in 6% efficient thermally annealed polymer photovoltaics. *Applied Physics Letters* **2007,** *90* (16), 163511.
58. Kim, Y.; Cook, S.; Tuladhar, S. M.; Choulis, S. A.; Nelson, J.; Durrant, J. R.; Bradley, D. D. C.; Giles, M.; McCulloch, I.; Ha, C.-S.; Ree, M., A strong regioregularity effect in self-organizing conjugated polymer films and high-efficiency polythiophene:fullerene solar cells. *Nature Materials* **2006,** *5* (3), 197-203.
59. Van Bavel, S. S.; Bärenklau, M.; de With, G.; Hoppe, H.; Loos, J., P3HT/PCBM Bulk Heterojunction Solar Cells: Impact of Blend Composition and 3D Morphology on Device Performance. *Advanced Functional Materials* **2010,** *20* (9), 1458-1463.

60. Wang, J.; Wang, D.; Moses, D.; Heeger, A. J., Dynamic quenching of 5-(2'-ethyl-hexyloxy)-p-phenylene vinylene (MEH-PPV) by charge transfer to a C60 derivative in solution. *Journal of Applied Polymer Science* **2001,** *82* (10), 2553-2557.
61. Bag, M.; Gehan, T. S.; Renna, L. A.; Algaier, D. D.; Lahti, P. M.; Venkataraman, D., Fabrication conditions for efficient organic photovoltaic cells from aqueous dispersions of nanoparticles. *RSC Adv.* **2014,** *4* (85), 45325-45331.
62. Al-Mudhaffer, M. F.; Griffith, M. J.; Feron, K.; Nicolaidis, N. C.; Cooling, N. A.; Zhou, X.; Holdsworth, J.; Belcher, W. J.; Dastoor, P. C., The origin of performance limitations in miniemulsion nanoparticulate organic photovoltaic devices. *Solar Energy Materials and Solar Cells* **2018,** *175*, 77-88.
63. Xie, C.; Classen, A.; Späth, A.; Tang, X.; Min, J.; Meyer, M.; Zhang, C.; Li, N.; Osvet, A.; Fink, R. H.; Brabec, C. J., Overcoming Microstructural Limitations in Water Processed Organic Solar Cells by Engineering Customized Nanoparticulate Inks. *Advanced Energy Materials* **2018**, 1702857.
64. Kesava, S. V.; Fei, Z.; Rimshaw, A. D.; Wang, C.; Hexemer, A.; Asbury, J. B.; Heeney, M.; Gomez, E. D., Domain Compositions and Fullerene Aggregation Govern Charge Photogeneration in Polymer/Fullerene Solar Cells. *Advanced Energy Materials* **2014,** *4* (11), 1400116.

Water-dispersed PTNT:$PC_{71}BM$ NPs prepared using a non-chlorinated solvent, *o*-xylene.

Using *o*-xylene leads to higher photovoltaic performance compared to using chloroform.

DMTA probes morphological change of NP film as a function of annealing temperature.

Thermal annealing to the complete device improves the device performance.